Atomistic Modeling of Amorphous Aromatic Polybenzoxazoles

Venkatesh J. Vasudevan and James E. McGrath*

Department of Chemistry, NSF Science and Technology Center for High Performance Polymeric Adhesives and Composites, Virginia Polytechnic Institute and State University, Blacksburg, Virginia 24061-0212

Received August 2, 1995; Revised Manuscript Received October 30, 1995[⊗]

ABSTRACT: Atomistic models of two different fluorinated polybenzoxazoles, 6F-PBO and 3F-PBO, were used to simulate the amorphous structures of these polymers. Molecular mechanics and molecular dynamics techniques were utilized to relax the independent structures from an initial high-energy system. The relaxed model structures showed 6F-PBOs to be more coiled relative to 3F-PBO. Conformational grid search was performed on each of the repeat units to analyze the local structure of the two polymeric backbones. The torsional angles corresponding to energy minima and rotational barrier were found to vary between the 6F and 3F structure due to differences in the pendant group at the C_α carbon atom. The Hildebrand solubility parameters and elastic constants for the two different polymers were estimated from simulation. 3F-PBO is predicted to possess a higher solubility parameter and higher moduli compared to the 6F-PBO.

Introduction

Aromatic heterocyclic polybenzoxazoles (PBO) **1** are a class of high-performance, high-T_g polymers that exhibit excellent thermal stability, high mechanical strength, and resistance to common solvents and are complementary to the polyimides **2**.

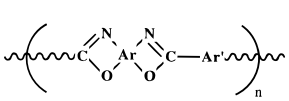

1

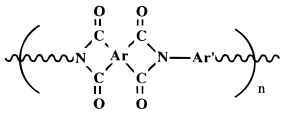

2

They may be synthesized in two steps[1,2] by the initial formation of poly(hydroxy amides) through polycondensation of bis(*o*-aminophenol) with aromatic diacid chlorides followed by thermal cyclization. They have potential uses as new electronic packaging materials, adhesives, polymer matrix resins, and gas permeation membranes. Over the past few years, rigid-rod poly(benzobisoxazoles) have been the object of interest in the preparation of high-performance films and fibers due to their excellent thermo-oxidative stability and exceptional tensile properties. Experimental investigations on the thermal, mechanical, and rheological properties of these polymers were reported in a series of publications.[3−5] Theoretical studies were directed at characterizing the limited conformational flexibility[6] about the *p*-phenylene group in each repeat unit and also the interchain interactions in the liquid or semicrystalline state of PBOs.[7] Semiempirical quantum mechanical analysis[8] showed that the *p*-phenylene ring was coplanar with the rigid oxazole unit as predicted earlier from a molecular mechanics study.[6] Recently, rotational isomeric state theory combined with molecular dynamics simulation of a single PBO chain in vacuum was used to evaluate the persistence length, a_∞, of these rigid polymers.[9]

The high strength and stability associated with these polymers are also known to produce undesirable characteristics such as low transverse strengths and unfavorable processing conditions. Several attempts were made to enhance the processability of these stiff polymers through better solubility at lower temperatures while retaining the oxidative stability of the heterocyclic aromatic units.[10−12] One of the methods of improving processability has been through the synthesis of fluorine-containing polybenzoxazoles[13−15] via step polymerization followed by thermal cyclodehydration. In particular, two different semirigid polybenzoxazoles,[16−18] **3** and **4**, have been synthesized by separately reacting each of the aminophenol monomers, (a) 2,2-bis(3-amino-4-hydroxyphenyl)-1,1,1,3,3,3-hexafluoropropane and (b) 1,1-bis(3-amino-4-hydroxyphenyl)-1-phenyl-2,2,2-trifluoroethane, with 4,4′-oxydibenzoyl chloride.

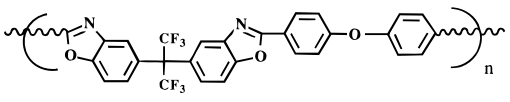

3

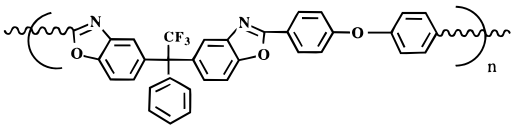

4

The resultant fluorinated amorphous polybenzoxazoles are designated as 6F-PBO (**3**) and 3F-PBO (**4**), indicating the number of fluorine atoms per repeat unit. The fibrous, off-white polymers displayed T_g values ranging between 280 (6F) and 300 °C (3F). They formed transparent and ductile films.[16−18] They also displayed high tensile strength, good thermo-oxidative stability, and enhanced solubility. In addition to their interest as gas permeation membranes, adhesives, and matrix resins, their optical properties are noteworthy.

Several experimental methods have been used to characterize the amorphous state of these polymers but some of the details are hard to achieve. In contrast, molecular modeling techniques provide atomic-level structural details such as chain conformation and packing in the bulk and free volume distribution in the amorphous polymer. An enormous increase in computing power combined with the availability of commercial software over the past few years has played a significant role in the utilization of molecular simulations to characterize several amorphous polymeric materials.[19−21]

[⊗] Abstract published in *Advance ACS Abstracts,* December 15, 1995.

0024-9297/96/2229-0637$12.00/0

The purpose of this work was to study the structures and static properties of novel amorphous polybenzoxazoles (6F-PBO and 3F-PBO) using molecular mechanics and molecular dynamics simulations.

The technique for the generation of amorphous bulk polymer at high density was developed and applied successfully by Theodorou and Suter.[19] They evaluated the static properties of glassy atactic polypropylene using energy minimization methods. Rigby and Roe[22,23] used molecular dynamics simulation in canonical ensemble (N,V,E) to produce the melt and glassy structure of short-chain alkanes. By reducing the simulated temperature in steps, they showed that the volume of their system increased and the dihedral angles of the bonds ceased to rotate, indicating a possible onset of T_g. Recently, Fan and Hsu[24] have applied Theodorou and Suter's approach to estimate the mechanical and thermal properties of polysulfones using a commercial software. Similar studies on other amorphous polymeric systems such as poly(vinyl chloride),[25] polybutadiene,[26] and polycarbonates[27] have shown unique structures and properties that compare well to experimental data.

The polybenzoxazole backbone may contain several common structural features such as bis-A type linkages and phenoxybenzene units present in commercial thermoplastic materials such as polysulfones and polycarbonates. However, the presence of pendant fluorine atoms and heterocyclic fused rings is unique to our fluorinated polybenzoxazole backbone, and hence their influence on the overall and local structures of these polymers should provide an interesting analysis. The simulation study discussed in this paper particularly focuses on generating two different (6F- and 3F-PBO) model amorphous polybenzoxazoles and determining the overall polymer structure and properties such as solubility parameter, density, and end−end distances. Special emphasis has also been placed on investigating the local structure of the polymers using the conformational grid search. The influence of the different side groups on the flexibility and average dimension of the polymers was also studied. Elastic constants such as the tensile and bulk modulus of the amorphous polymers were also determined using molecular mechanics. The simulations were conducted on a Stardent-750 workstation using the commercial software Polygraf (version 3.2.1), distributed by Molecular Simulations Inc.

Simulation Details

The monomer repeat units of the polybenzoxazoles are shown in **3** (6F) and **4** (3F). The degree of polymerization in our simulation model was set equal to 10 for both the 6F- and 3F-PBO. Explicit hydrogens were used in both model systems, bringing the total number of atoms in the 10-mer system to 542 (6F) and 612 (3F). The bulk amorphous state was simulated using periodic boundary conditions with an initial density of 1.30 g/cm^3 at 300 K. The amorphous polymer chain was generated using a Monte Carlo method[19] for random assignment of dihedral angles on the polymer backbone. Generation of the initial amorphous structures was dependent on the allowable minimum distance, which was equal to the sum of the van der Waals radii of the nonbonded atoms. As new monomer units were added to the backbone of the growing chain, the nonbonded distances of the atoms were checked for overlaps and only distances smaller than the minimum were allowed. However, if a newly grown atom resulted in overlap energies, then that new atom placement was rejected and other dihedral angles were tried in a random fashion until the allowed distance was obtained for that atom. If an acceptable conformation was not obtained after several such attempts, then the algorithm deleted a few previously assigned atoms and started growing the chain from that point in a fresh manner. The van der Waals radii of atoms were scaled down to 30% of their original value to avoid overlaps while the polymers were packed to a high density initially. After the completion of the packing, the van der Waal radii of the atoms were brought to their original value, resulting in high repulsive energy.

The structures were relaxed initially by energy minimization using the conjugate-gradient method with Ewald summation. In all these calculations, the total potential energy E was calculated as the sum of various energy contributions as follows:

$$E = E_{\text{bond stretch}} + E_{\text{bond bend}} + E_{\text{torsion}} + E_{\text{inversion}} + E_{\text{vdW}} \quad (1)$$

The Dreiding force field[28] contains different functional forms for each of the above-mentioned energy terms, and the following definitions were adopted:

$$E_{\text{bond stretch}} = [0.5K_{\text{bs}}(R - R_{\text{o}})^2] \quad (2a)$$

$$E_{\text{bond bend}} = [0.5K_{\text{bb}}(\theta - \theta_{\text{o}})^2] \quad (2b)$$

$$E_{\text{torsion}} = [0.5K_{\text{t}}(1 - \cos\{n(\varphi - \varphi_{\text{o}})\})] \quad (2c)$$

$$E_{\text{inversion}} = [0.5K_{\text{inv}}(\psi - \psi_{\text{o}})^2] \quad (2d)$$

$$E_{\text{vdW}} = AR^{-12} - BR^{-6} \quad (2e)$$

The subscript "o" indicates equilibrium values, and K's denote the force constants for specific interactions. Van der Waals distance and energy parameters for nonbonded interactions between heteronuclear atoms were obtained by arithmetic mean and geometric mean, respectively, of the individual atomic parameters. The reader is referred to the original paper on the Dreiding force field[28] for values, definitions of the terms, and symbols used in the above expressions. Atomic charges were not included in our nonbonded energy calculations. The generic Dreiding force field parameters widely applied in polymer simulation[9,24] were derived based on crystalline structures of small organic and inorganic molecules. The simplicity of a general force field such as the Dreiding force field, while convenient when applied to any new combination of atoms, may lead to lower accuracy for a specialized subset of molecules. However, bulk simulation of a polymer with C, H, N, O, and F atoms should lead to reasonably accurate predictions because the Dreiding force field is optimized well for small molecules with this given set of atoms. The Dreiding force field can also be limited in simulation of bulk thermodynamic properties such as isothermal compressibility.

A straightforward molecular mechanics scheme is likely to trap the simulated system in a metastable local high-energy minima. Molecular dynamics simulation was used to prevent the system from such entrapments by providing thermal energies to cross energy barriers between local minima. The standard Verlet[29] algorithm was used to integrate Newton's law of motion with a

Table 1. Average Internal Stress Tensors (in MPa) of Model Polybenzoxazoles

stress tensor	3F-PBO	6F-PBO
σ_{xx}	-0.13 ± 0.46	-0.46 ± 1.15
σ_{xy}	0.20 ± 1.13	-0.07 ± 0.91
σ_{xz}	-0.22 ± 0.34	0.13 ± 0.29
σ_{yy}	0.22 ± 0.50	-0.23 ± 0.42
σ_{yz}	0.17 ± 0.48	-0.52 ± 0.51
σ_{zz}	-0.18 ± 0.21	0.43 ± 0.75

time step of 0.001 ps. For the canonical N,P,T dynamics,[30] the relaxation time constant τ and the masslike parameter which determines the rate of change of volume/shape matrix were set to 0.1 ps and 1.00, respectively. Each molecular dynamics run was started by assigning initial velocity for the atoms according to a Boltzmann distribution at 600 K. The velocities of the atoms were quickly scaled down so that the final temperature of atoms was 300 K. The total external pressure was maintained at 1 atm, and Nose's algorithm[31] was used to keep the cell temperature constant at 300 K in the molecular dynamics simulation. The pressure and temperature used in our simulation are convenient computational parameters to relax the model polymer and are not intended to reproduce the actual thermodynamic state (P,V,T) of the real polybenzoxazoles. In the past, molecular dynamics simulations[22,23] have been used to obtain thermodynamic properties such as density and the internal energy of model polymer systems by time averaging the properties over a long duration ($\sim$500 ps) run. Our purpose in using short-run molecular dynamics in this investigation is to relax the bulk structure efficiently by introducing thermal motions to cross any energy barriers between local minima. The cell volume fluctuations during our N,P,T dynamics simulation reduced the computational time required to obtain a well-relaxed structure.

A relaxation cycle consisted of a 10 ps dynamics run followed by an energy minimization run, and several such cycles (about 5−7) were applied to each amorphous structure generated. The convergence criteria used for energy minimizations was a root-mean-square (rms) force less than 0.1 (kcal/mol)/Å for the polymer and 0.1 (kcal/mol)/Å^3 for the stresses on the periodic boxes. Both convergence criteria were simultaneously satisfied for the system to be relaxed completely. The simulation box was allowed to vary in size and shape during both the energy minimization and molecular dynamics in order to find the equilibrium density for each structure.

Results and Discussion

Six independent structures for each of 6F- and 3F-PBO polymers were generated according to the procedure detailed above. The properties reported here are ensemble averaged from the appropriate set of six structures. Table 1 lists the average values of six internal stress tensors in the simulation boxes at the end of equilibration. The internal stress components, σ_{ij}, are defined as the first derivative of the potential energy per unit volume with respect to strain. At equilibrium these values must be close to zero, and any high positive or negative values indicate the system to be under tension or compression. Table 1 shows the internal stress in units of MPa, and the very low values suggest that the polymer structures are indeed well relaxed. The simulation cell parameters were allowed to vary during the relaxation, and the average cell dimensions from each set of six final structures are presented in Table 2. The amorphous structures cannot be considered to be totally isotropic because of small deviations of the cell from cubic dimensions.

Table 2. Average Cell Dimensions of the Relaxed Structures

cell dimension	3F-PBO	6F-PBO
a (Å)	20.77 ± 1.48	20.75 ± 2.21
b (Å)	20.33 ± 0.95	19.01 ± 1.50
c (Å)	20.25 ± 1.74	21.93 ± 2.10
α (deg)	88.39 ± 11.17	90.98 ± 8.73
β (deg)	89.90 ± 4.19	87.21 ± 5.14
γ (deg)	86.28 ± 6.32	90.32 ± 8.13

Table 3. Ensemble-Averaged Energies of Equilibrated Amorphous Structures [kcal/mol (structure)]

energy	3F-PBO	6F-PBO
bond stretching	171.25 ± 2.29	136.64 ± 0.76
bond bending	405.03 ± 11.12	392.76 ± 3.18
torsional	133.31 ± 21.33	112.99 ± 9.61
inversion	6.54 ± 2.11	4.16 ± 0.85
van der Waals (bulk)	374.03 ± 25.29	320.88 ± 26.07
total	1090.17 ± 32.72	967.36 ± 26.34
van der Waals (isolated)	751.63 ± 18.95	620.54 ± 8.55

The optimum densities of the 6F- and 3F-PBO polymers were found to be 1.11 ± 0.04 (6F) and 1.14 ± 0.03 (3F) g/cm^3. These densities are somewhat lower than the experimental values of 1.20 ± 0.02 g/cm^3 determined for both the polymers. Such lower values of densities have been predicted from simulation studies on other amorphous polymers such as polysulfones[21,24] and polycarbonates.[27] The final model structures are generated at 0 K because the energy minimization technique does not include thermal motions of atoms. The molecular dynamics simulation introduces the temperature effect but is too short to calculate equilibrium time-averaged density and is intended only to quicken the relaxation process. One way to avoid this density discrepancy is to generate amorphous polymer structures at a constant experimental density value at a known temperature.[26] However, the relaxation of such structures with fixed cubic volume leads to higher stresses (40−100 MPa) on the simulation boxes. Polymer structures with semirigid benzoxazole units produced even higher stresses when the box size and shape were not allowed to vary and generally required a large number of relaxation cycles. In such cases, increasing the temperature in a constant-volume molecular dynamics did not aid in the overall relaxation of the structure. On the other hand, varying the cell parameters during the relaxation relieves the stresses ($\sim$1−2 MPa) albeit resulting in lower densities. Fan and co-workers[27] have studied the effects of initial density on chain packing in model polycarbonates. They found that final densities were closer to the experimental values at room temperature if the specified initial densities were higher than or equal to the known density at 300 K. The chain building was easier when a lower initial density was used but the final structures did not pack more densely, however. A systematic error in the final densities of the polymer structures was attributed to the force field parameters optimized against the crystal structures near room temperature rather than at 0 K.

The total potential energy and their compositions for the polybenzoxazole structures are presented in Table 3 for the 6F- and 3F-PBO polymers. The small deviations in the energetic components and their sum ($\sim$3%) for the different structures indicate that the amorphous polymers are well equilibrated. Bond-stretch and bond-angle bending energies are very nearly constant and are also major contributors to the total energy of the

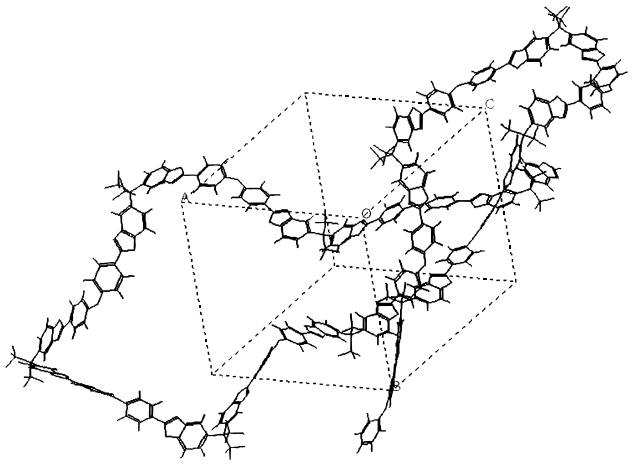

Figure 1. Simulated model of an amorphous 3F-PBO structure.

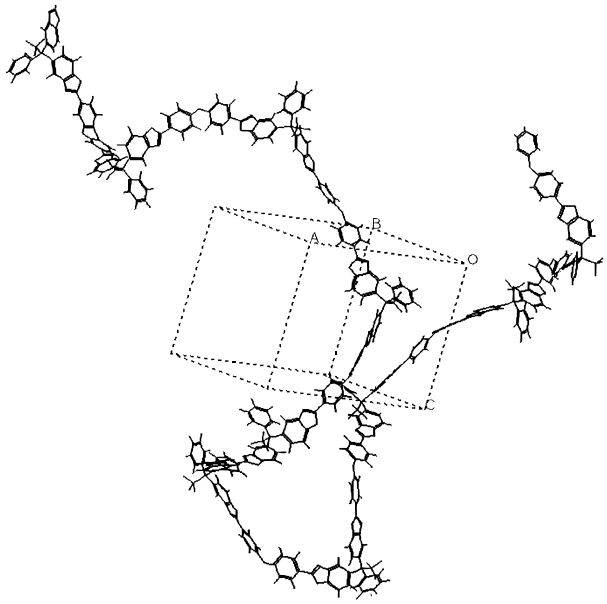

Figure 2. Simulated model of an amorphous 6F-PBO structure.

structures. A direct comparison of the energies between the 6F- and 3F-PBO structure is not valid because the total number of atoms and interactions in the parent chain for each type of PBO is different. The standard deviation values listed in Table 3 show that the fluctuations in the torsional and van der Waals potentials are considerably higher than the other energetic components. Figures 1 and 2 show representative model structures of the 6F- and 3F-polybenzoxazoles, respectively. The structures of the polymers shown in these figures are among several available to an amorphous state of the polymer at that density. The boxes show the volume occupied by the polymer at the equilibrium condition. The distinct feature of these structures is the planar nature of the benzoxazole unit due to fusion of the five-membered oxazole ring with the phenyl unit resulting in conjugation. The average $C_{(Ph)}-C_{\alpha}-C_{(Ph)}$ bond angle values are found to be 108.7 ± 1.5 (6F) and $110.0 \pm 4.6°$ (3F). The two phenyl rings on either side of the backbone oxygen are nonplanar with an average value of $124.4 \pm 7.6°$ for the $C_{(Ph)}-O-C_{(Ph)}$ bond angle. These average bond angle values are reasonable for such moieties and indicate that the relaxation steps did not result in unusual bond bendings.

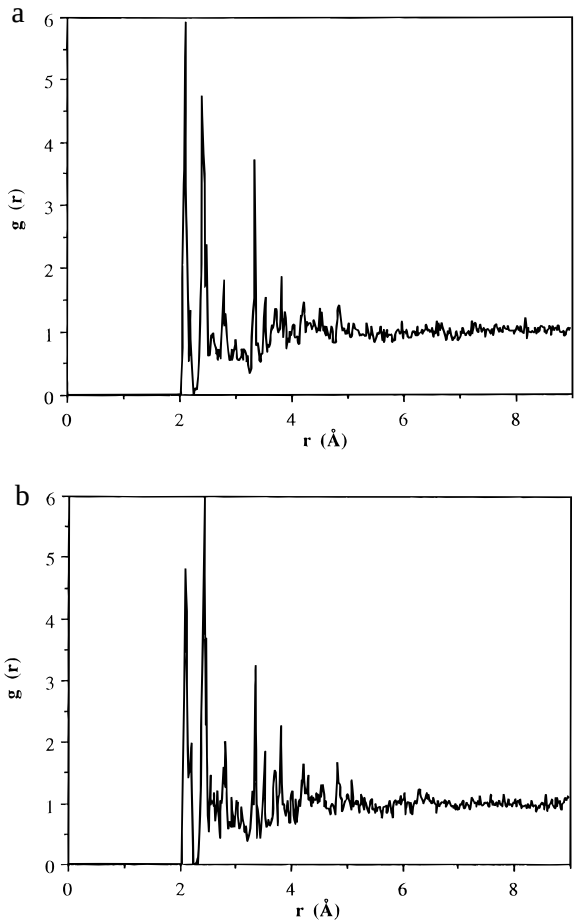

Figure 3. Averaged radial distribution functions for the relaxed polybenzoxazoles: (a) 3F-PBO; (b) 6F-PBO.

Radial Distribution Function. The absence of long-range order distinguishes an amorphous structure from its crystalline state. The pair correlation function or radial distribution function (RDF) gives a measure of the order in the system by computing the average spatial configuration of the atoms. The RDF can easily be calculated from simulation and is also related to the structure factor accessible experimentally from X-ray diffraction. The pair correlation function can be defined as the probability of finding any two atoms separated by distance r, relative to the probability of finding two atoms at a distance r apart in an ideal gas at the same density. Since our model contains different atoms, a full set of all the pair correlations between atoms is required to completely characterize the system. However, the total radial distribution function which does not account for the difference in the atom type can be used to examine the features of amorphous nature in an average fashion. The RDF averaged from six different structures for the 6F- and 3F-PBOs are shown in Figure 3.

The intermolecular RDF for distances less than 2.0 Å is not plotted. The peaks at distances less than 2.0 Å arise due to chain connectivity and can be assigned to covalently bonded atoms. For example, C−H and C−C bonds of phenyl rings give sharp peaks around 1.08 Å (peak values ~35.1 from this calculation) and 1.36 Å. Peaks that occur at distances greater than 2.0 Å are generally due to nonbonded atoms separated by two (1−3), three (1−4), and four (1−5) bonds on the connected chain. This structural order due to intramolecular connections disappears at about 5.0 Å. At distances farther than 5.0 Å, there are no peaks, indicating a total absence of order. The RDFs for the 6F- and 3F-PBOs

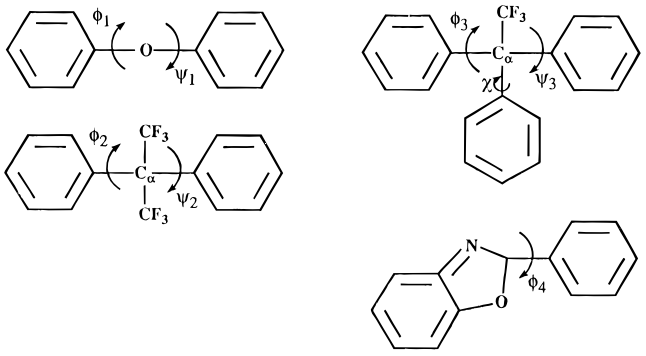

Figure 4. Definitions of torsional angles used in the conformational grid search analysis of 6F-PBO and 3F-PBO monomers.

show peaks at similar distances below 5.0 Å. The peak heights at any distance r denote the relative concentration of atoms within a sphere of radius equal to r. Parts a and b of Figure 3 show slight variations in the peak heights at distances 2.1 and 2.4 Å, indicating the local structural differences between the two type of polybenzoxazoles. For example, the distance between the nonbonded carbons and hydrogens separated by two bonds in a phenyl ring is about 2.1 Å and since the 3F-PBO contains more of such pairs relative to the 6F-PBO, the RDF for the 3F-PBO shows a higher peak at this distance. Other correlations such as fluorine and hydrogens of the substituent phenyls at the C_α atom also occur at distances of about 2.4 Å. These local structural differences are manifested by relative peak heights at these distances.

Conformational Characteristics. The conformational freedom of rotation for the backbone bonds is an important factor in determining the local structure, flexibility, and average dimensions of the polymer. The extent of rotation and energy barrier to rotation are also influenced by the pendant groups on the polymer backbone. Conformational grid search allows one to vary simultaneously the torsional angles of successive bonds and plot the total energy as a contour value against each pair of rotational angles. The potential energy contour plot thus derived indicates not only the possible chain conformation but also the chain relaxation pathways. For the conformational grid search, the torsional angles along the backbones are defined as in Figure 4, and the calculations were performed using just one repeat unit of the polybenzoxazoles. The interaction energies were calculated by varying the backbone torsional angles ϕ and ψ at intervals of 10° and minimizing the structure like keeping the torsions of the concerned pair of bonds fixed. In the case of phenyl substituent at the C_α carbon atom in 3F-PBO, for each of the (ϕ_3,ψ_3) states the angle χ was not varied separately during energy minimizations. However, we believe that the phenyl pendant group is optimized during energy minimizations to be at its lowest energy position corresponding to that particular (ϕ_3,ψ_3) state.

The contributions to the total energy include rotational terms, bond stretching terms, bending terms, and nonbonded interactions. The potential energy contour plots are shown in Figures 5−7. The energy difference between each contour line is 1.0 kcal/mol and is indicated in these figures relative to the local energy minima denoted by + sign. For the C−O rotations, the minima are located symmetrically near (±30°,±30°), and the energy barrier between local minima is about 4.0 kcal/mol. The conjugative effect tends to stabilize

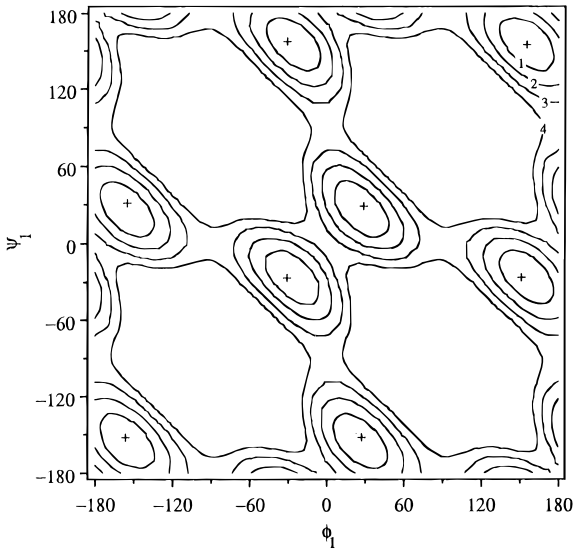

Figure 5. Potential energy contour map as a function of the rotations of angles ϕ_1 and ψ_1. Energy differences between contour lines are equal to 1 kcal/mol.

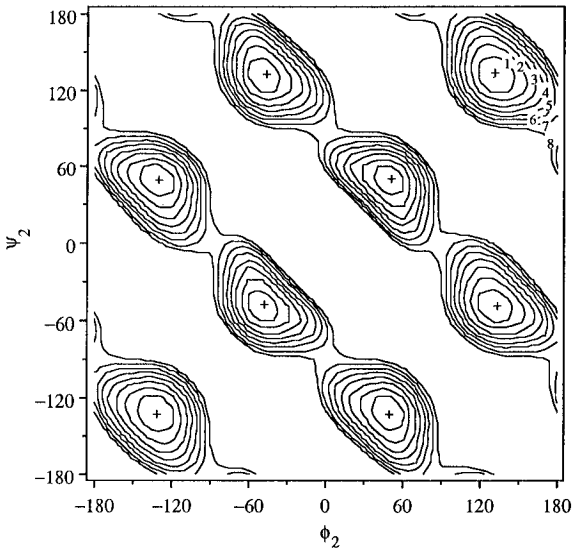

Figure 6. Potential energy contour map as a function of the rotations of angles ϕ_2 and ψ_2 when substituents at the C_α carbon atom are CF_3 and CF_3. Energy differences between contour lines are equal to 1 kcal/mol.

the coplanar conformation of the phenyl rings due to maximum overlap of the π electrons of oxygen and phenyl. However, in the coplanar conformation, the ortho hydrogens on the phenyls overlap, leading to a high energy. Therefore the twist conformation represents a balance between opposing forces of conjugation and repulsion due to hydrogen overlap in a coplanar conformation. Our result compares favorably with other conformational studies[32] on diphenyl ether linkages showing a twisted conformation of phenyls with a distinct minimum near (±40°,±40°) and an energy barrier of only 3 kcal/mol. Experimental data on polymer crystals[33] with such linkages also confirm twisted minimal conformations. The slight variations in the location of minima between our results and earlier investigations can be attributed to a wider C−O−C bond angle of 128° found in our monomer structure compared to 123 ± 2° from other studies.[32]

A previous study of diphenyl ether linkages using the Dreiding force field predicted the local minima to be at (±90°,±90°) (Figure 6 of ref 21). It was also reported

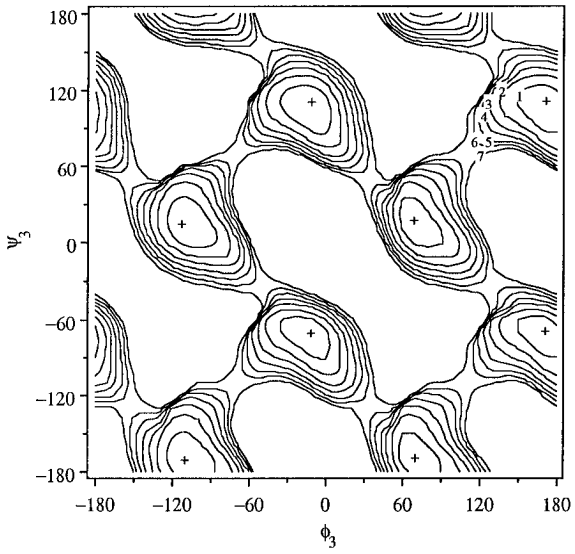

Figure 7. Potential energy contour map as a function of the rotations of angles ϕ_3 and ψ_3 when substituents at the C_α carbon atom are CF_3 and phenyl. Energy differences between contour lines are equal to 1 kcal/mol.

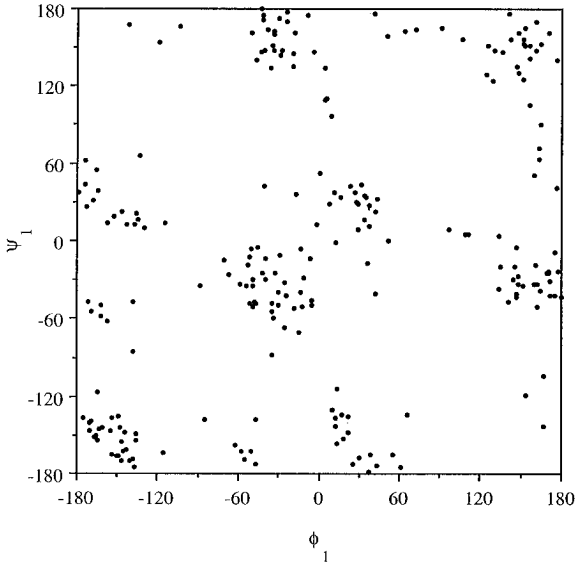

Figure 8. Actual distribution of dihedral rotations ϕ_1 and ψ_1 from the backbone of the amorphous structures of both 3F- and 6F-PBO. The plots are overlaid.

that similar dihedral distributions were found in their relaxed amorphous polysulfone structures. Our experience with the Dreiding force field indicates that such energy maps could be produced when the bonds connecting the oxygen to two phenyl rings are hybridized as sp^3 instead of a resonant structure. The difference lies in the equilibrium bond angle of these species, 104.1° (sp^2 or sp^3) and 120° (resonance), as specified in the Dreiding force field. The torsional potential barrier to rotation is only 2.0 kcal/mol for sp^3 bonds compared to the 25.0 kcal/mol for the resonant bonds. The smaller bond angle for sp^3 oxygen brings the hydrogens in the phenyls too close and hence twists the phenyls into perpendicular planes with minima at ±90.0°. Recently, Fan et al.[27] have made similar observations about the oxygen connecting the carbonate carbon and phenylene in polycarbonates. They modified the bond bending and torsional potential terms in the Dreiding force field for the oxygen to fit *ab initio* data of model compounds while recognizing the hybridization effects.

Figure 6 shows the symmetrical conformational map for $C_{(Ph)}-C_\alpha-C_{(Ph)}$ linkages in 6F-PBO and predicts the local minima at (±50°,±50°) with an energy barrier of about 7.5 kcal/mol. The $C_{(Ph)}-C_\alpha-C_{(Ph)}$ bond angle of the model compound after optimization was equal to 109.1°. This group is therefore considered very rigid, and in the favorable conformation, the two phenyls and six fluorines of the CF_3's are interlocked. Transitions between minima occur along a low-energy path only by synchronous rotations of bonds ϕ_2 and ψ_2 in such a fashion that one increases and the other decreases. Conformational energy maps with two CF_3 substituents at the C_α atom have been studied by Anwer and co-workers,[32] who predicted local minima at (±46°,±46°). The energy barrier calculated from their study is 2.5 kcal/mol lower than our results. Also a crystal structure[34] containing such linkages showed conformations with torsional angles at minima of (±42.3°,±42.3°).

Figure 7 shows the conformational energy map for rotational angles ϕ_3 and ψ_3 in the 3F-PBO structure. It is clear that the minima are locally restricted at (±10°,-70°) and the torsional barrier is also raised to 6.5 kcal/mol. When Figures 6 and 7 are superpositioned, the domains within the 6.0 kcal/mol energy in the latter bridged similar domains in Figure 6. The isoenergy contour of the 7.0 kcal/mol spans a broad range of conformations that are connected both in the "antidiagonal" and "diagonal" direction. This means that synchronous motion of the angles ϕ_3 and ψ_3 takes place, with both angles increasing when they are connected in the diagonal direction. We are not aware of any conformational studies on model compounds with CF_3 and phenyl substituents at the C_α atom. However, Figure 7 is similar to the conformational map plotted by Sundararajan[35] for the polycarbonate chain segment with CH_3 and phenyl substituent at the C_α carbon atom. In our model studies, the rotational angle χ of the substituent phenyl group was not optimized separately, however. The overall similarity in the optimal geometries and rotational energy barriers calculated from our conformational studies and previous studies on similar moieties[32,35] demonstrates that the generic Dreiding force field leads to reasonable structure predictions.

The actual torsional angle distributions calculated from each set of six relaxed amorphous polymer structures are plotted in Figures 8−10. The $C_{(Ph)}-O-C_{(Ph)}$ torsional distributions from the 6F- and 3F-PBO polymers were similar to each other and are therefore overlaid in Figure 8. The dihedral angle distributions for the C−O rotations are wide, spreading over a large area with a maximum concentration near ±30°. Distributions of the $C_{(Ph)}-C_\alpha$ rotations in the case of 6F-PBO, shown in Figure 9, are restricted around the local minimum values found from the conformational study. However, the $C_{(Ph)}-C_\alpha$ rotations in 3F-PBO, presented in Figure 10, are delocalized and span a broader range of continuous conformations similar to the conformational energy map in Figure 7. It is quite easy to see that some of the actual conformations are at higher energy (3−4 kcal/mol) according to Figure 7. This does not mean that the amorphous structures still contained very high energy conformations. The difference between Figures 7 and 10 arises due to small bond-angle distortions present in the amorphous structures. Such small bond bending reduces the torsional barrier and allows some of the amorphous polymer backbone to assume higher energy conformations predicted with fixed bond angles on the model compound. The spread of torsional angles can also be due to initial packing density and

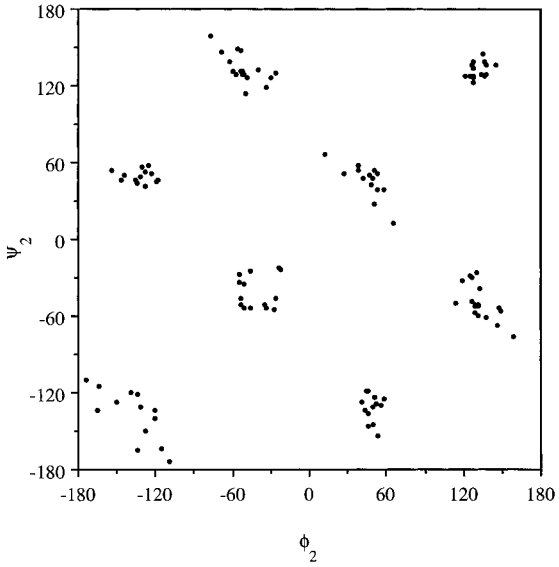

Figure 9. Actual distribution of dihedral rotations ϕ_2 and ψ_2 from the backbone of the amorphous structures of both 3F-PBO structures.

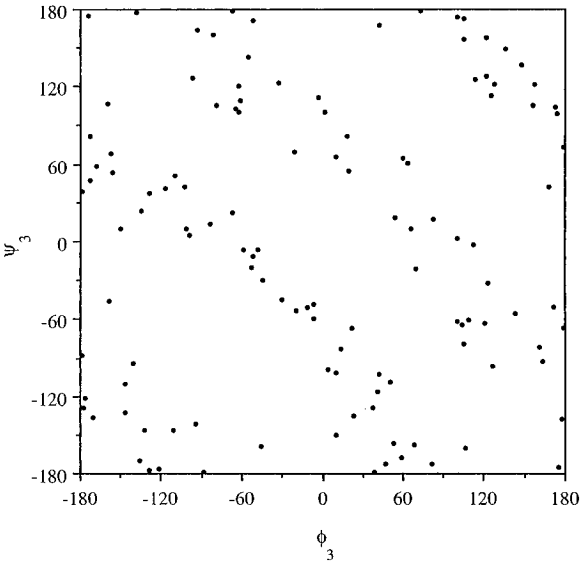

Figure 10. Actual distribution of dihedral rotations ϕ_3 and ψ_3 from the backbone of the amorphous 6F-PBO structures.

subsequent relaxations. However, the overall similarity between the dihedral distributions in the simulated amorphous structures and the model compounds indicates that the polymers are well relaxed locally and the effect of the initial density on the microstructure of the polymers is minimal.

The planarity of the *p*-phenylene unit attached to the oxazole unit in the trans and cis PBO has already been investigated by Mark and co-workers.[6,8] The coplanar conformation was expected to be favored due to resonance stabilization and better packing. Figure 11 shows the actual rotational distributions of the $C-C_{(Ph)}$ bond, connecting the oxazole and the phenylene, calculated from our 12 amorphous polybenzoxazole structures. Due to symmetry reasons, the range of torsional angles studied is between 0 and 90°. The distribution peaks are near 0 ± 10°, indicating that the majority of the phenylene rings are coplanar with the oxazole units. The distribution is rough due to statistics from a small but finite number of data from our simulations.

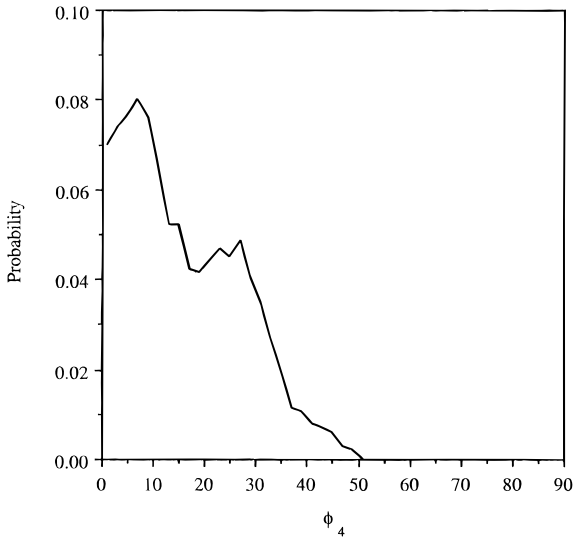

Figure 11. Actual probability distribution of dihedral rotations ϕ_4 from the backbone of the amorphous 3F- and 6F-PBO structures.

Characteristic Ratio. The characteristic ratio is defined as the ratio of the square of the end-to-end distances of a given polymer to that of an ideal Gaussian chain. For an ideal chain, the square of the end-to-end distance is equal to nl^2, where n is the number of structural segments in the backbone and l is the length of that structural unit. The characteristic ratio is thus equal to

$$C_n = \langle r^2 \rangle_0 / nl^2 \tag{3}$$

and is a measure of chain flexibility. Equation 3 assumes a single structural unit with constant length in the polymer backbone. For an ideal flexible chain, C_n is equal to 1.00, indicating a fully coiled polymer. For polymer backbones that contain different structural units as in our fluorinated polybenzoxazole, it is convenient to assume virtual bonds of two types, $C-C_6H_3-NO-C$ and $C-C_6H_4-O$, with lengths equal to 5.97 and 5.76 Å, respectively. For the purposes of calculation of the C_n, a value of l equal to the average of the two structural unit lengths, 5.87 Å, was used. Such an approach has been previously applied to estimate the characteristic ratio of polysulfones.[21] Each of our model polymers contained a total of 40 virtual bonds. The average end-to-end distance for the 3F- and 6F-PBOs were 63.0 ± 23.6 and 54.8 ± 21.2 Å, respectively. The root-mean-square end-to-end distances, $(\langle r^2 \rangle)^{1/2}$, were 66.2 (3F) and 59.0 Å (6F). The characteristic ratios were calculated to be 3.18 (3F) and 2.52 (6F), indicating that the 3F-PBO polymer is more stiff relative to 6F-PBO. This is due to the differences in the pendant groups at the C_α carbon atom in the two different fluorinated polymers. These results compare to a C_n of 2.11 predicted for polysulfones,[21] 1.79 for polycarbonates,[35] and about 6.0 for polyimide[36] while the experimental values generally range between 4 and 10.0 for most commercial polymers.

Hildebrand Solubility Parameter. The Hildebrand solubility parameter, δ, is defined as the square root of the cohesive energy density. Cohesive energy is defined as the increase in internal energy per mole of the substance when all intermolecular forces are eliminated. Cohesive energies can be obtained from simulation by calculating the difference between the energies

Table 4. Ensemble-Averaged Properties of Polybenzoxazoles

property	unit	3F-PBO	6F-PBO
density	g/cm^3	1.14 ± 0.03	1.11 ± 0.04
characteristic ratio		3.18	2.52
E_{coh}	kcal/mol	377.6 ± 51.6	299.7 ± 34.9
molar volume	cm^3/mol	4961.6 ± 220.6	4951.3 ± 453.63
solubility parameter	(cal/cm^3)$^{1/2}$	8.73 ± 0.45	7.72 ± 0.71

of the periodic structure and an isolated parent chain. Thus

$$E_{coh} = E_{isolated} - E_{periodic} \quad (4)$$

The Hildebrand solubility parameter is simply the square root of the cohesive energy density

$$\delta = (E_{coh})/V)^{1/2} \qquad (cal/cm^3)^{1/2} \quad (5)$$

where V is the molar volume in cm^3/mol. Table 3 lists the energies of the bulk and isolated chains ensemble averaged over the six related structures. The cohesive energy densities calculated according to eq 4 for the two fluorinated polybenzoxazoles are listed in Table 4. The average molar volume for the two types of model polymers are 4961.6 ± 220.6 (3F) and 4951.3 ± 453.63 cm^3 (6F). The solubility parameter, δ, is then calculated to be 8.73 ± 0.45 (3F) and 7.72 ± 0.71 (6F) (cal/cm^3)$^{1/2}$.

The difference in the solubility parameter between the two types of PBO is essentially due to E_{coh}, because the molar volumes of 3F- and 6F-PBO are nearly the same. It is difficult to compare directly the E_{vdW} energies of the 3F- and 6F-PBO chains because of their different atomic compositions. However, it can be understood that the positive repulsive energy of the isolated chain is depressed when similar chains surround them in the bulk. This reduction in the total energy raises solely due to the intermolecular nonbonded attractive interactions between the atoms from neighboring chains in the bulk. Such favorable energetic interactions "solvate" the chain, and this effect is predicted to be higher for 3F-PBO relative to 6F-PBO. The planar pendant phenyl ring in the case of 3F-PBO allows more solvation atoms from other surrounding chains to access the backbone atoms compared to the tetrahedral CF_3 group in the case of 6F-PBO. This does not necessarily mean that the 3F-PBOs are packed better because the densities of both types of PBOs are similar. The planarity of the substituent phenyl ring rather than the density is the main reason for the improved solvation found in 3F-PBO relative to 6F-PBO. Experimental values are not known exactly although both polymers dissolved in solvents with δ >9.0 (cal/cm^3)$^{1/2}$ such as tetrahydrofuran (THF), chloroform, *N*-methylpyrrolidinone (NMP), and *o*-dichlorobenzene.[18] Experiments also showed that the 3F-PBOs were more soluble than their 6F counterparts, although the influence of molecular weights of the polymer samples on the solubility was not clear.

Elastic Constants. The elastic constants for amorphous PBOs can be calculated by deforming the equilibrated model structures generated. Typically, small strains are applied to the simulation box and the amorphous polymer is subsequently energy minimized, leading to new internal stresses within the simulation cell. The change in the internal stress tensor subject to the applied strain is used to generate a "stiffness matrix" followed by determination of various elastic constants. This scheme is called the static method of estimating the elastic constants and has been successfully applied to polysulfone[24] and polycarbonate[27] systems. In contrast to this, Brown and Clarke[37] have adopted a dynamic method of calculating the mechanical properties. In their study, constant-stress molecular dynamics simulation was performed to determine the strain to calculate the "compliance matrix" and modulus. This method has been criticized for time-consuming calculations and large fluctuations of the strain with time. In this study, the static method of estimation has been adopted.

The mechanical properties of these amorphous polymers were estimated from the stiffness matrix determined while applying external strain to the simulation box. The components of the stiffness matrix can be defined by

$$C_{ij} = \partial\sigma_i/\partial\epsilon_j = (\sigma_{i+} - \sigma_{i-})/2\epsilon_j \quad (6)$$

where σ_i and ϵ_j are the stress and strain components, respectively (i,j = 1, 2, ..., 6). The subscripts "+" and "−" denote the stresses under extensive and compressive strains. For a simple cubic cell, applying a desired external strain involves changing only one of the six cell parameters. The cell parameters for each of the optimized amorphous polybenzoxazoles in this study correspond to a triclinic system. In this case, applying a strain in the x direction (ϵ_1) requires changing not only a but also b, c, α, β, and γ. A general method for applying strain to a nonsymmetric simulation cell has recently been developed by Fan et al.[27] In this study, such a scheme was utilized for calculating the stiffness matrix with an applied strain of 0.05% (5.0×10^{-4}).

The calculated stiffness matrix averaged for each of the six independent (6F- and 3F-PBO) polybenzoxazole structures is shown below.

$$\begin{array}{cc} \text{6F-PBO} & \text{3F-PBO} \\ \begin{pmatrix} 5.94 & 2.26 & 3.94 & 0.66 & -0.38 & 0.00 \\ 3.10 & 5.78 & 2.94 & 0.48 & -0.10 & 0.90 \\ 3.28 & 3.22 & 6.16 & 1.04 & 0.90 & -0.98 \\ 0.50 & 1.20 & 0.50 & 1.50 & 0.04 & 0.70 \\ -0.56 & -0.46 & -0.86 & 0.02 & 1.72 & 0.72 \\ -0.30 & -0.32 & -0.18 & 0.20 & 0.22 & 1.54 \end{pmatrix} & \begin{pmatrix} 8.13 & 3.70 & 3.35 & 1.48 & 1.32 & 0.05 \\ 3.75 & 7.57 & 3.45 & -0.27 & 0.78 & -0.53 \\ 3.05 & 2.37 & 7.45 & -0.40 & -0.18 & 0.15 \\ -1.70 & -1.20 & -0.68 & 2.30 & -1.85 & -0.73 \\ 1.30 & 1.48 & -0.23 & 0.28 & 2.45 & -0.10 \\ -0.05 & 0.98 & 1.08 & 0.30 & 0.68 & 2.5 \end{pmatrix} \end{array} \quad (7)$$

This matrix is compared to the idealistic matrix associated with an isotropic amorphous state

$$\begin{pmatrix} \lambda+2\mu & \lambda & \lambda & 0 & 0 & 0 \\ \lambda & \lambda+2\mu & \lambda & 0 & 0 & 0 \\ \lambda & \lambda & \lambda+2\mu & 0 & 0 & 0 \\ 0 & 0 & 0 & \mu & 0 & 0 \\ 0 & 0 & 0 & 0 & \mu & 0 \\ 0 & 0 & 0 & 0 & 0 & \mu \end{pmatrix} \quad (8)$$

where λ and μ are Lame's constants. For isotropic material, the stiffness matrix should be symmetrical, i.e., $C_{ij} = C_{ji}$. However, as shown in eq 6, the C_{ij} and C_{ji} are obtained using different deformation paths and also the limitations in the energy minimization method to reach a global minimum lead to a nonsymmetric C_{ij}. Nevertheless, the basic features of an isotropic material are shown by similar values in the principal diagonal terms (C_{11}, C_{22}, C_{33}) and the three shear moduli (C_{44}, C_{55}, C_{66}). The terms which are expected to be zero for an ideal isotropic material are much smaller than the nonzero terms. The Young's modulus, shear modulus, bulk modulus, and Poisson ratio are derived from the

Table 5. Average Elastic Constants of Model 3F- and 6F-Polybenzoxazoles

elastic constant	6F-PBO	3F-PBO
Lame's constant, λ	3.09 ± 0.23 (GPa)	3.21 ± 0.34 (GPa)
shear modulus, μ	1.53 ± 0.24 (GPa)	2.25 ± 0.78 (GPa)
Young's modulus, E	4.53 ± 0.30 (GPa)	6.24 ± 1.30 (GPa)
bulk modulus, B	4.28 ± 0.56 (GPa)	4.58 ± 0.95 (GPa)
Poisson ratio, ν	0.33 ± 0.02	0.31 ± 0.08

Lame constants as follows and are listed in Table 5 for both 3F- and 6F-PBO.

$$\text{Young's modulus } (E) = \mu\frac{3\lambda + 2\mu}{\lambda + \mu} \tag{9a}$$

$$\text{bulk modulus } (B) = \lambda + \frac{2}{3}\mu \tag{9b}$$

$$\text{Poisson ratio } (\nu) = \frac{\lambda}{\lambda + \mu} \tag{9c}$$

The predicted values indicate that 3F-PBO has a higher overall modulus compared to 6F-PBO. The tensile moduli of uncured films made from end-capped 6F-PBO polymers of different molecular weights have been measured to be in the range 2.3−5.3 GPa.[38] The predicted Young's modulus for 6F-PBO compares very well to the experimental values considering that the unreacted end cap would not alter the thermoplastic properties significantly. For most of the glassy polymers, Poisson's ratio is in the range 0.33−0.38 and the values predicted for the PBOs are quite acceptable.

Conclusions

The use of molecular modeling techniques allows for the generation of equilibrium, stress-free structures of two different fluorinated amorphous polybenzoxazole polymers with varied pendant groups at the C_α atom. These structures did not exhibit long-range order, indicating an amorphous state as shown from their RDFs. The torsional angle distributions for the polymer backbone compared well with the conformational map of model compounds, indicating a well-relaxed amorphous structure at short ranges. The barrier for the $C-C_\alpha$ rotations were higher relative to the more flexible C−O rotations. 6F-PBO was found to be relatively flexible compared to 3F-PBO. The Hildebrand solubility parameters calculated for the two types of fluorinated benzoxazole indicate that 3F-PBO was more soluble than its 6F counterpart as observed experimentally. The calculated densities were slightly lower for both types of PBOs, and this was generally attributed to the force field parameters, which were not optimized to produce accurate thermodynamic properties such as isothermal compressibility for polymers.

Acknowledgment. The authors appreciate the support of the National Science Foundation Science and Technology Center (Contrast No. DMR-20004) and the Gas Research Institute (Contrast No. 5891-222 2303). Molecular Simulations Inc. is gratefully acknowledged for providing the Polygraf (version 3.2.1) software.

References and Notes

(1) Kubota, T.; Nakanishi, R. *J. Polym. Sci., Part A* **1965**, *3*, 2107.
(2) Imai, Y.; Taoka, I.; Uno, K.; Iwakura, Y. *Makromol. Chem.* **1965**, *83*, 167.
(3) Wolfe, J. F.; Arnold, F. E. *Macromolecules* **1981**, *14*, 909.
(4) Choe, E. W.; Kim, S. N. *Macromolecules* **1981**, *14*, 920.
(5) Chu, S. G.; Venkatraman, S.; Berry, G. C.; Einaga, Y. *Macromolecules* **1981**, *14*, 939.
(6) Welsh, W. J.; Bhaumik, D.; Mark, J. E. *Macromolecules* **1981**, *14*, 947.
(7) Bhaumik, D.; Welsh, W. J.; Jaffe, H. H.; Mark, J. E. *Macromolecules* **1981**, *14*, 951.
(8) Yang, Y.; Welsh, W. J. *Macromolecules* **1990**, *23*, 2410.
(9) Zhang, R.; Mattice, W. L. *Macromolecules* **1992**, *25*, 4937.
(10) Evers, R. C.; Arnold, F. E.; Helminiak, T. E. *Macromolecules* **1981**, *14*, 925.
(11) Chow, A. W.; Bitler, S. P.; Penwell, P. E.; Osborne, D. J.; Wolfe, J. E. *Macromolecules* **1989**, *22*, 3514.
(12) Hilborn, J. G.; Labadie, J. W.; Hedrick, J. L. *Macromolecules* **1990**, *23*, 2854.
(13) Reinhardt, B. A. *Polym. Commun.* **1990**, *31*, 453.
(14) Maruyama, Y.; Oishi, Y.; Kakimoto, M.; Imai, Y. *Macromolecules* **1988**, *21*, 2305.
(15) Khanna, D. N.; Mueller, W. H. *Proc. Photopolym., Principles, Processes, Mater.* **1988**, 429.
(16) Joseph, W. D.; Abed, J. C.; Mercier, R.; McGrath, J. E. *Polymer* **1994**, *35*, 5046.
(17) Joseph, W. D.; Mercier, R.; Prasad, A.; McGrath, J. E. *Polymer* **1993**, *34*, 866.
(18) Joseph, W. D. Ph.D Thesis, Virginia Polytechnic Institute and State University, 1993.
(19) Theodorou, D. N.; Suter, U. W. *Macromolecules* **1985**, *18*, 1467.
(20) Boyd, R.; Pant, P. V. K. *Macromolecules* **1991**, *24*, 4078.
(21) Fan, C. F.; Hsu, S. L. *Macromolecules* **1991**, *24*, 6244.
(22) Rigby, D.; Roe, R. J. *J. Chem. Phys.* **1987**, *87*, 7285.
(23) Rigby, D.; Roe, R. J. *J. Chem. Phys.* **1988**, *89*, 5280.
(24) Fan, C. F.; Hsu, S. L. *Macromolecules* **1992**, *25*, 266.
(25) Ludovice, P. J.; Suter, U. W. *Computational Modeling of Polymers*; Bicerano, J., Ed.; Marcel Dekker: New York, 1992.
(26) Li, Y.; Mattice, W. L. *Macromolecules* **1992**, *25*, 4942.
(27) Fan, C. F.; Cagin, T.; Chen, Z. M.; Smith, K. A. *Macromolecules* **1994**, *27*, 2383.
(28) Mayo, S. L.; Olafson, B. D.; Goddard, W. A., III. *J. Phys. Chem.* **1990**, *94*, 8897.
(29) Verlet, L. *Phys. Rev.* **1967**, *159*, 98.
(30) Parinello, M.; Rahman, A. *Phys. Rev. Lett.* **1981**, *52*, 7182.
(31) Nose, S. J. *Mol. Phys.* **1984**, *52*, 255.
(32) Anwer, A.; Lovell, R.; Windle, A. H. *Computer Simulation of Polymers*; Roe, R. J., Ed.; Prentice-Hall: Englewood Cliffs, NJ, 1991.
(33) Boon, J.; Magre, E. P. *Makromol. Chem.* **1969**, *126*, 130.
(34) Shklover, V. E.; Struchkov, Y. T.; Dzhanashvili, M. M.; Vaseav, V. A. *J. Gen. Chem. USSR (Engl. Transl.)* **1980**, *50*, 2075.
(35) Sundararajan, P. R. *Macromolecules* **1989**, *22*, 2149.
(36) Zhang, R.; Mattice, W. L. *Macromolecules* **1993**, *26*, 6100.
(37) Brown, D.; Clarke, J. H. R. *Macromolecules* **1991**, *24*, 4073.
(38) Joseph, W. D.; Abed, J. C.; Yoon, T. H.; McGrath, J. E. *Polym. Prepr. (Am. Chem. Soc., Div. Polym. Chem.)* **1994**, *35* (1), 551.

MA951133L